# Estimating Coarse 3D Shape and Pose from the Bounding Contour

Paria Mehrani and James H. Elder
*Department of Electrical Engineering and Computer Science, York University, 4700 Keele Street, Toronto, Canada*
*paria@cse.yorku.ca, jelder@yorku.ca*

Keywords: Shape Estimation, 3D Shape Reconstruction, Single-view Reconstruction, Shape-from-contour.

Abstract: Single-view reconstruction of a smooth 3D object is an ill-posed problem. Surface cues such as shading and texture provide local constraints on shape, but these cues can be weak, making it a challenge to recover globally correct models. The bounding contour can play an important role in constraining this global integration. Here we focus in particular on information afforded by the overall elongation (aspect ratio) of the bounding contour. We hypothesize that the tendency of objects to be relatively compact and the generic view assumption together induce a statistical dependency between the observed elongation of the object boundary and the coarse 3D shape of the solid object, a dependency that could potentially be exploited by single-view methods. To test this hypothesis we assemble a new dataset of solid 3D shapes and study the joint statistics of ellipsoidal approximations to these shapes and elliptical approximations of their orthographically projected boundaries. Optimal estimators derived from these statistics confirm our hypothesis, and we show that these estimators can be used to generate coarse 3D shape-pose estimates from the bounding contour that are significantly and substantially superior to competing methods.

## 1 INTRODUCTION

To be clear on terminology, we follow (Koenderink, 1984) and refer to the set of surface points grazed by the view vector as the *rim* of the object, and the projection of these points into the image as the *occluding contour*.

It is well known that the occluding contour strongly constrains surface shape at the rim (Koenderink, 1984). Indeed, human judgement of surface shape is strongly influenced by the shape of the occluding contour (Todd and Reichel, 1989; Todd, 2004), and often even the occluding contour alone provides a compelling sense of volumetric shape (Tse, 2002; Elder, 2014) (Fig. 1). Understanding the information provided by the occluding contour is important not only for this limiting case, but also for devising algorithms that effectively exploit contour cues in conjunction with (possibly weak) surface cues such as shading and texture (Karsch et al., 2013).

Figure 1: Volumetric shape from the bounding contour.

While the computer vision literature on shape from contour is relatively small, there have been a few interesting studies in recent years exploring the degree to which solid shape can be reconstructed from occluding contours alone (Igarashi et al., 1999; Twarog et al., 2012; Karsch et al., 2013). These studies have tended to focus on extracting a complete, detailed model of the 3D shape from the boundary, without considering whether the solution will be close to correct at a global scale. Here we take the opposite view, and ask whether the bounding contour can tell us anything about the *global shape* of the object at the coarsest scale and its 3D pose. If this global information can be estimated from the bounding contour, it could then be used to help constrain algorithms that recover more detailed 3D structure so that reconstructions are correct at both *local* and *global* scales.

Most computer vision work in this area exploits the bounding contour in conjunction with surface cues within an optimization framework. Typically, user interaction and/or some inflation term in the objective function are required to avoid a trivial (flat) solution. Users were required to specify depth of some surface points in (Prasad et al., 2006), or a fixed volume that the shape must fill in (Toppe et al., 2011). Oswald (Oswald et al., 2009) used an inflation term.

More recent studies has avoided user interaction



Mehrani P. and Elder J.
Estimating Coarse 3D Shape and Pose from the Bounding Contour.
DOI: 10.5220/0006190306030610
In *Proceedings of the 12th International Joint Conference on Computer Vision, Imaging and Computer Graphics Theory and Applications (VISIGRAPP 2017)*, pages 603-610
ISBN: 978-989-758-225-7

and arbitrary inflation terms and instead have combined local surface shading cues with contour information to estimate surface shape. Cole (Cole et al., 2012) estimate local surface normals within an MRF framework and fit a final 3D surface to the estimated normals using a thin plate spline. Barron and Malik (Barron and Malik, 2015) assume a probabilistic framework, imposing a prior over the variation in mean surface curvature. While both of these systems fuse shading and contour cues to determine the reconstruction, Karsch (Karsch et al., 2013) have shown that internal contour cues appear to be stronger cues to shape than shading.

A very different strategy for single-view estimation of smooth solid shapes was first introduced in the interactive sketching interface dubbed Teddy (Igarashi et al., 1999) and later studied by Twarog (Twarog et al., 2012) under the pseudonym *Puffball*. (We will use the latter term as an evocative label for this class of methods.) In this approach, the solid shape is defined as the envelope of spheres centred on the interior skeleton (Blum, 1973) of the shape in the image, and bi-tangent to the occluding contour (Fig. 2). The method is simple and can produce surprisingly reasonable results in many cases.

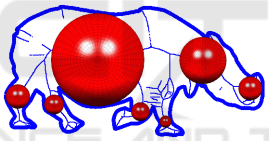

Figure 2: Puffball reconstruction (Twarog et al., 2012).

One limitation of all of these prior algorithms is that they are typically constrained or at least strongly biased to return a planar or near-planar and fronto-parallel rim (i.e., a frontal pose), whereas in the real world under general viewing the probability of this is vanishing. A second potential problem is that these methods impose strong constraints or priors on the overall depth of the objects. For example, by defining solid shape as an envelope of spheres, Puffball makes a very strong local symmetry assumption: at every point on the skeleton, the depth of the object (dimension in the viewing direction) is equal to twice the distance of the contour from the skeleton. Are these assumptions reasonable?

One of the difficulties in answering this question is that most prior work has been evaluated only qualitatively, not quantitatively. Important exceptions are the work of Karsch (Karsch et al., 2013) and Barron & Malik (Barron and Malik, 2015), however their evaluations do not explicitly test these assumptions.

## 2 OUR CONTRIBUTIONS

Instead of focusing on detailed shape reconstruction, our goal in this paper is to understand information afforded by the bounding contour on the rough shape and global 3D pose of the object. In particular, we wish to understand whether the contour can provide a cue to the rough length, width and depth of the object, and how it might be angled out of the fronto-parallel plane. To address this question we will study the joint statistics of ellipsoidal approximations of real scanned objects and their image projections. Here we confine ourselves to orthographic projection, under which these ellipsoidal approximations generate elliptical images.

Our specific contributions are:

1. We introduce a new dataset and methodology for evaluating methods for single-view reconstruction of smooth solid objects.
2. We show that statistically, even a simple elliptical approximation of the occluding contour provides substantial information about the coarse 3D shape and pose of the object.
3. We show that the assumptions of symmetry in depth and fronto-parallel pose imposed by prior work lead to large errors in single-view 3D object estimation.

## 3 INTUITION

Why would a simple elliptical approximation to the occluding contour carry information about 3D shape and pose? One of our intuitions is rooted in the compactness of real objects. While objects vary widely in shape, we conjecture that extreme elongations are relatively rare. This has implications when we observe an elongated occluding contour in the image (Fig. 3(a)).

There is an infinite family of solid objects that could have generated this contour. However, if the longest dimension of the object is angled away from fronto-parallel, the object must be even more elongated than the occluding contour. This induces a bias for elongated occluding contours to project from objects whose long dimension is close to fronto-parallel, whereas for less elongated contours the long dimension is relatively more likely to be angled away from the image plane.

A second intuition derives from the generic viewpoint assumption (Freeman, 1994). Imagine an elongated object with its longest dimension in the viewing direction (Fig. 3(b)). A small change in 3D pose

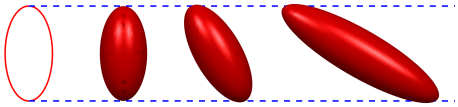

(a) Ellipsoids of various shapes can give rise to the same ellipse. The ellipse is viewed from front while ellipsoids are viewed from top.

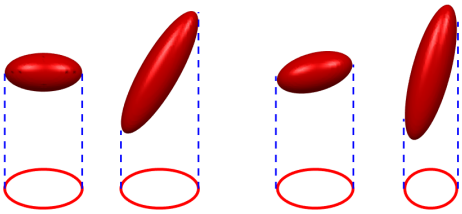

(b) Two ellipsoids giving rise to the same ellipse with and without fronto-parallel poses (left), and same ellipsoids rotated 15 deg. The projection of the longer ellipsoids has drastic changes with small perturbations in pose (right).

Figure 3: Top: An infinite family of shapes can project onto the same contour. Bottom: Drastic changes in projection of an elongated ellipsoid with small perturbations in its pose.

will induce a large change in the appearance of the occluding contour. If, on the other hand, the object is rotated so that its smallest dimension is in the viewing direction, the same change in 3D pose will induce a relatively small change in the occluding contour. This suggests that the expected extent of the object in depth may be small relative to the dimensions observed in the image, counter to the Puffball assumption.

These are only qualitative intuitions. The main point of this paper is test these intuitions quantitatively, using a simple sampling technique.

## 4 DATASET

At time of writing, we are not aware of any large-scale public collection of real 3D scanned objects. For the purposes of this project, we have therefore assembled a collection from various sources on the internet including the BigBIRD dataset (Singh et al., 2014), the YCB object and model set dataset (Çalli et al., 2015), and various other 3D model sharing websites such as Sketchfab[1]. Any duplicates were removed. The final dataset consists of 122 objects, which we randomly divided into training and test sets of 61 objects each. Some examples are shown in Fig. 4.

[1]https://sketchfab.com.

Figure 4: Example 3D objects in our dataset.

## 5 METHODS

### 5.1 Priors

We employ ellipsoids as low-order 3D models capturing global shape and pose. We first use an iterative closest point algorithm (Besl and McKay, 1992) to determine, for each object in the dataset, the ellipsoid that minimizes mean squared Euclidean error (Figures 12 and 13). The size and shape of each ellipsoid is completely characterized by the length of its three axes: $a \geq b \geq c$. Since we are not concerned with absolute size, we can collapse these three numbers into two ratios specifying the length of its two smaller axes relative to the largest axis: $1 > \lambda_2 = b/a > \lambda_3 = c/a > 0$ . The collection of ellipsoid fits to our training data then form our *empirical shape prior* (Fig. 6(a)).

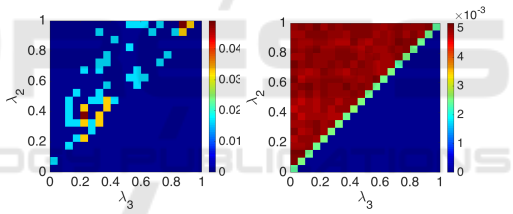


Figure 5: Ellipsoid shape priors. Left: Empirical prior derived from training objects. Right: Theoretical prior, based on a uniform distribution of axis lengths.

There are two major limitations of this prior. First, given the limited size of our dataset, it is of course quite noisy. Second, since we employed opportunity sampling to form the dataset, it is certain to contain bias. For these reasons, we also constructed a theoretical *uniform shape prior*, formed by sampling triplets of numbers uniformly on $[0,1]$, scaling each triplet to have maximum value 1, and then assigning the middle and smaller values to $b$ and $c$. As expected, the resulting distribution is uniform on the subspace $\lambda_2 \geq \lambda_3$. (The green diagonal stripe reflects the fact that only half of each bin on the diagonal lies in the feasible subspace.) Note that the mean of this distribution is $(\lambda_2 = 2/3, \lambda_3 = 1/3)$. In other words, the mean shape under the uniform prior has axes in the ratio $3:2:1$.

While the limited sample size for the empirical prior makes detailed comparison with the uniform prior difficult, we can at least make some qualitative observations. First, the empirical prior seems to

be biased somewhat toward more compact, less elongated ellipsoids, i.e., toward $\lambda_2 = \lambda_3 = 1$. Second, there appears to be a bias toward the diagonal, i.e., toward $\lambda_2 = \lambda_3$, which represents the family of prolate spheroids (cigar shapes).

We assume a uniform prior over 3D pose. The 3D pose can be characterized by the angle $\theta_1$ and $\theta_2$ of the two larger ellipsoid axes with respect to the view vector (Fig 6), as the remaining degree of freedom induces a rotation in the projected ellipse, but does not change its shape.

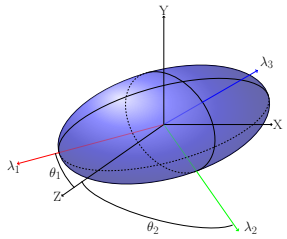


Figure 6: The angles $\theta_1$ and $\theta_2$ characterize the 3D pose of ellipsoid.

## 5.2 Likelihoods

To learn the joint statistics of coarse 3D object shape/pose and occluding contour shape, we sampled ellipsoids from the 3D shape/pose priors and projected them (orthographically) as ellipses to the image. For both empirical and uniform priors we randomly sampled 1 million shape/pose combinations. Again, the ellipse shape is completely characterized by the ratio $0 < m < 1$ of the length of the minor to the major axis. The result is a five-dimensional joint ellipsoid-ellipse space $(\lambda_2, \lambda_3, \theta_1, \theta_2, m)$. To analyze the joint distribution, we partitioned the space into 20 bins in each dimension, resulting in 3.2 million bins. With only 1 million samples, this discrete space will be sparsely populated overall. However in practice the density is far from uniform, so that most estimators can be calculated with reasonable accuracy.

We consider three estimation problems:

1. Estimation of ellipsoid shape (marginalizing over pose).
2. Estimation of ellipsoid pose (marginalizing over shape).
3. Joint estimation of ellipsoid shape and pose.

We will consider three distinct estimators for ellipsoid shape and pose given an ellipse shape:

1. Puffball. To represent the strategy employed by symmetry axis methods, (Igarashi et al., 1999; Twarog et al., 2012) the ellipsoid is assumed to be a prolate spheroid with longest axis in the image plane and matching the major axis of the ellipse and the other two smaller axes matching the minor axis of the ellipse ($\lambda_2 = \lambda_3 = m$).
2. Maximum a Posteriori (MAP). The most probable ellipsoid shape/pose is selected.
3. Minimum Mean Squared Error (MMSE). The ellipsoid shape/pose minimizing the expected squared error is selected. We define the error as the symmetric mean Euclidean distance between points on estimated and ground truth ellipsoids.

For the joint estimation of ellipsoid shape and pose, the MMSE solution is computationally expensive to compute and we therefore approximate it with a Mean estimator, which selects the ellipsoid with mean shape/pose parameters. We also consider a Puffball solution that selects a random pose, for reasons explained below.

Recall that all three estimation problems are ill-posed: each estimator proposes an ellipsoid shape and/or pose that is consistent with the observed ellipse (Within some tolerance due to the discrete sampling of shape and pose parameters.) Differences in the ellipsoid estimates may thus reflect only a) knowledge of the 3D shape/pose prior, b) an understanding of how projection affects the joint statistics of the ellipse and generating ellipsoid and/or c) loss function (delta function for MAP, quadratic for MMSE and Mean).

Fig. 7 shows the resulting estimators for shape and Fig. 8 shows estimators for pose. Note that in the Puffball solution the largest axis is always in the image plane ($\theta_1 = 90$ deg), and that $\lambda_2 = \lambda_3 = m$.

Consider first the estimation of shape. Regardless of prior and whether we are doing marginal or joint estimation, the MAP solution follows Puffball fairly closely. However, the MAP solution for shape does deviate slightly from Puffball, and these deviations are important (see below). A more profound divergence from Puffball is seen in the MMSE and Mean shape solutions, which in general return a losenge rather than a cigar for all ellipses, with the two smaller axes differing substantially in length.

Further insight can be gained by considering the estimation of pose. Due to sampling error the MAP solution is noisy, but it can be clearly seen that, unlike Puffball, the major axis of the ellipsoid is slanted away from the image plane by between 15 and 75 deg. Note that, to be consistent with the observed ellipse, this means that at least one of the smaller ellipsoid axes must be slightly smaller than the puffball prediction, a condition which can be verified from Fig. 7.

In the case of MMSE/Mean estimators, unlike Puffball, the major axis of the ellipsoid does not tend to lie in the image plane ($\theta_1 = 90$ deg), but rather is angled out of the image plane by roughly 30 deg on

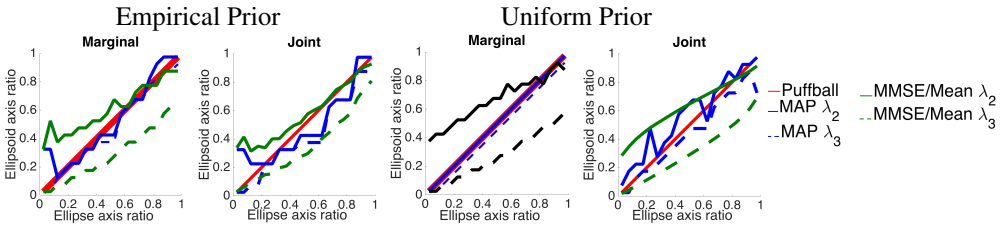


Figure 7: Estimators for shape.

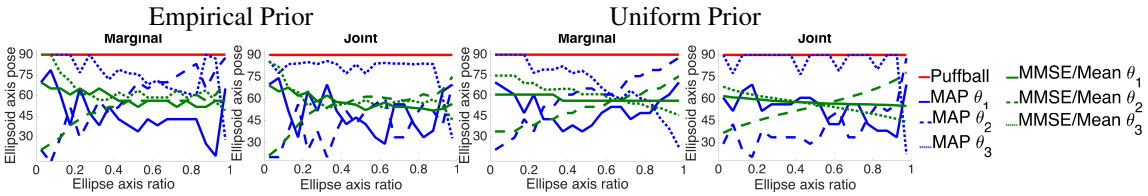


Figure 8: Estimators for pose.

average ($\theta_1 = 60$ deg). This is not too surprising, as a uniform pose distribution (not conditioned on the observation of ellipse) generates an average value for $\theta_1, \theta_2$ and $\theta_3$ of 1 radian (about 57 deg).

More interesting is the fact that the angle of the major axis depends upon the ellipse shape: the major axis of the ellipsoid is closer to the image plane for more elongated ellipses. This is consistent with the intuitions we expressed above. Since the empirical prior favours compact shapes, a highly elongated ellipse is more likely to be generated by an ellipsoid whose major axis is closer to the image plane. Note, however, that we also see a variation, though smaller, for the uniform prior. This may be due to the generic view assumption: when conditioned on an image measurement (in this case, an ellipse), a highly elongated ellipsoid with major axis closer to the image plane is favoured as it makes the observation more stable with respect to angular perturbation, and thus generates a higher conditional probability density.

There is even larger variation in the angle of the second and third ellipsoid axes as a function of the shape of the ellipse. For small ellipse ratios, the third axis lies closer to the image plane, but for larger ellipse ratios the second axis lies closer to the image plane. This makes sense because highly elongated ellipses are more likely to be observed if the smallest ellipsoid axis is close to the image plane, whereas less elongated ellipses are more likely to be observed if the second axis is close to the image plane.

# 6 QUANTITATIVE EVALUATION

We have seen that the MAP, MMSE and Puffball estimators make quite distinct predictions of ellipsoid shape and pose from an observed ellipse. How does this relate to the perception of more complex objects?

Suppose a more complex occluding contour is observed. To obtain a rough estimate of 3D object shape and pose, we could first approximate this shape by an ellipse and then use one of these estimators to infer an ellipsoidal approximation of the 3D object, and/or its pose. But which should we use?

To answer this question, we sampled 200 random 3D poses for each of the 61 shapes in our test dataset, projected each to the image and used an ICP algorithm to compute the best-fitting ellipse to each observed occluding contour. We used each of our methods to estimate an ellipsoidal approximation of the original generating object from this observed ellipse.

We evaluated these ellipsoidal approximations by computing the bidirectional mean-squared Euclidean error between the estimated ellipsoid and the best-fitting ellipsoid for the ground truth object.

## 6.1 Shape Estimators

To evaluate the marginal shape estimators, each estimated ellipsoid was scaled and rotated to minimize the Euclidean distance from the ground truth ellipsoid, and the resulting mean symmetric Euclidean distance was used as a measure of error. Fig. 9 reveals that both MAP and MMSE shape estimators perform better than Puffball, with MMSE performing best.

While the overlapping standard error bars in the top panels of Fig. 9 might call into question the statistical significance of these differences, these variations in error are highly correlated across estimators. This correlated error can be factored out by considering the average *reduction* in error for each test shape for the MAP and MMSE estimators *relative* to Puff-

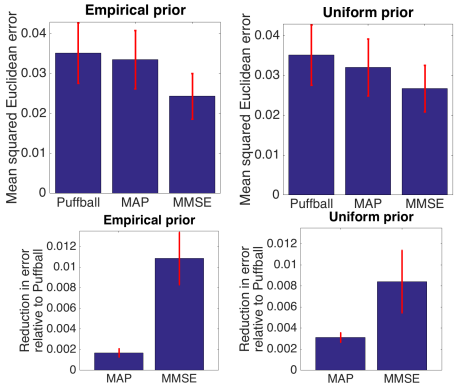


Figure 9: Top: Mean Euclidean error for marginal shape estimation. Bottom: ***Reduction*** in error relative to Puffball (larger is better).

ball (lower panels). From these plots it is easy to see that the reduction in error is highly significant for both MAP and MMSE. Table 1 shows the percent **reduction** in mean error and also the percentage of shapes for which error was lower for MAP and MMSE relative to Puffball. For MAP the improvement is relatively modest (5-9%) but consistent: MAP is better than Puffball for 75-97% of shapes. For MMSE the mean improvement is more substantial (24-31%) but less consistent: MMSE is better than Puffball for only 55-67% of shapes.

## 6.2 Pose Estimators

To evaluate the marginal pose estimators, we measured mean symmetric Euclidean error between ground truth ellipsoid at the correct and estimated poses. A problem emerges here: in our orthographic projection framework, for each ellipsoid there are four 3D 'metamer' poses that generate the same ellipse. To handle this, when an estimator generates a pose, we use an oracle to convert this to select from these four metamers the pose that generates minimal error relative to ground truth. Unfortunately, this puts Puffball at a disadvantage, since it represents a degenerate case where the four poses collapse to a single one. To address this, we add as a baseline a random pose estimator (Random), which selects a random pose, identifies the four metamers and then selects the optimal pose of these four using an oracle as described above.

As shown in Fig. 10, both MAP and MMSE pose estimators perform better than both Puffball and Random pose estimators. Since the Random estimator performs better than Puffball, we evaluate the performance of MAP and MMSE estimators relative to the latter (Fig. 10, bottom panels and Table 2.) Both MAP and MMSE generate significantly more accurate pose estimates. While MAP generates slightly greater mean improvement, improvements are more consistent across objects for MMSE.

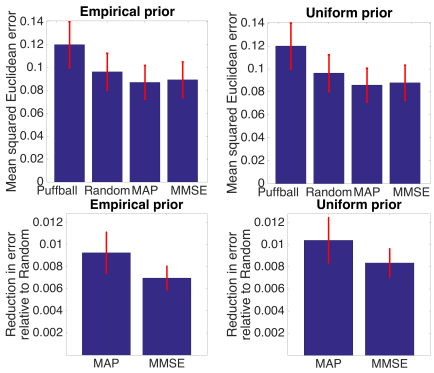


Figure 10: Top: Mean Euclidean error for marginal pose estimation. Bottom: ***Reduction*** in error relative to the Random pose estimator (larger is better).

## 6.3 Joint Configuration Experiments

For the joint estimators, symmetric Euclidean error of each estimated ellipsoid relative to the ground truth ellipsoid is computed, with no scaling or rotation. Again, an oracle is used to select the pose that yields lowest error, and this does put Puffball at a disadvantage. Unfortunately it is difficult to correct for this for joint shape-pose estimation, as selecting a random pose but using the Puffball shape would no longer be consistent with the observed ellipse. We therefore present results without correction, noting that the marginal shape and pose results presented above confirm that our MAP and MMSE estimators outperform Puffball for both of these dimensions individually.

Fig. 11 shows that for the empirical prior, the Mean estimator is best, while for the uniform prior, MAP and Mean are comparable. Table 3 shows that

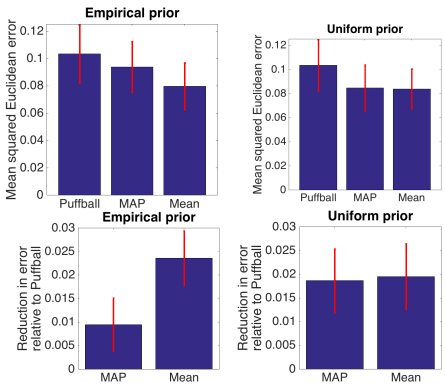


Figure 11: Mean Euclidean error for joint estimation. Bottom: ***Reduction*** in error relative to Puffball (larger is better).

the Mean estimator generates a greater average im-

Table 1: Performance of MAP and MMSE shape estimators relative to Puffball.

| Prior | Mean reduction in error | | % of objects for which error is reduced | |
|---|---|---|---|---|
| | MAP | MMSE | MAP | MMSE |
| Empirical | 5% | **31%** | **75%** | 67% |
| Uniform | 9% | **24%** | **97%** | 55% |

provement for the Empirical prior, but the MAP estimator is more reliable for the uniform prior.

Table 3: Performance of MAP and MMSE joint shape-pose estimators relative to Puffball.

| Prior | Mean reduction in error | | % of objects for which error is reduced | |
|---|---|---|---|---|
| | MAP | Mean | MAP | Mean |
| Empirical | 9% | **23%** | **70%** | 70% |
| Uniform | 18% | **19%** | **87%** | 67% |

## 7 QUALITATIVE EVALUATION

To get a qualitative sense of the performance of our joint shape-pose estimators, Figs. 12-13 show representative results for specific shapes in our test dataset, using MAP and Mean estimators based on our empirical prior. To generate Fig. 12, we first sorted the test cases by percent reduction in mean error for MAP over Puffball, and then show 0th, 25th, 50th, 75th and 100th percentile examples. The first (0th percentile) case is the shape for which MAP performs worst relative to Puffball. The last (100th percentile) case is the shape for which MAP has the largest error reduction relative to Puffball. The third (50th percentile) case is the median (representative) example. Similarly, Fig. 13 compares the Mean solution to Puffball.

In these qualitative comparisons, we note the elliptical projections of the estimated ellipsoids do not exactly match, and are sometimes quite different from the elliptical projections of the ground truth ellipsoids. This is primarily because the estimated ellipsoids are conditioned on an ellipse fitted in the image plane to the projected object, and in general this ellipse is different from the elliptical projection of the ground truth ellipsoid.

In addition, for a given shape there are small variations between the elliptical projections of the estimated ellipsoids. This is due to the finite sampling of shape and pose space.

Despite these limitations, the qualitative results are interesting. It is probably most instructive to consider the median results (third row) as these are representative. In both cases of Fig. 12 and 13, the statistical estimators have smaller errors relative to Puffball. Interestingly, in Fig. 13, the Mean estimator is able to capture the greater elongation and out-of-plane rotation of the object that Puffball is unable to capture.

Table 2: Performance of MAP and MMSE pose estimators relative to the Random pose estimator.

| Prior | Mean reduction in error | | % of objects for which error is reduced | |
|---|---|---|---|---|
| | MAP | MMSE | MAP | MMSE |
| Empirical | **10%** | 7% | 87% | **98%** |
| Uniform | **11%** | 9% | 92% | **98%** |

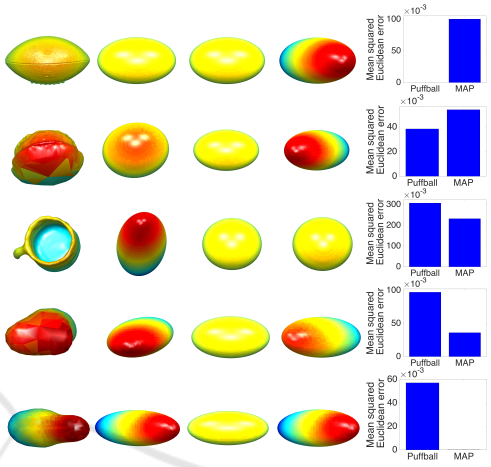


(a) Object (b) Ground truth (c) Puff-ball (d) MAP (e) Error

Figure 12: Examples of joint shape-pose estimation on test set objects. Objects were ranked according to the percent reduction in mean error for MAP over Puffball estimator. From top to bottom: 0, 25, 50, 75, and 100 percentile objects.

## 8 CONCLUSIONS AND FUTURE WORK

In this paper we set out to understand whether coarse 3D shape information could be extracted from object silhouettes even under orthographic projection. In particular, we conjectured that the tendency for objects to be compact and the generic view assumption should together bias the rough shape and pose when conditioned on the silhouette. Our experimental results confirm this hypothesis.

One limitation of this study is the use of an oracle to distinguish between four metamer poses in marginal pose and joint shape-pose estimations.

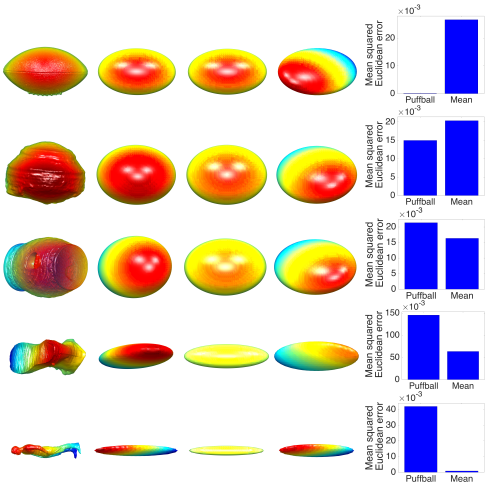


(a) Object (b) Ground truth (c) Puffball (d) Mean (e) Error

Figure 13: Examples of joint shape-pose estimation on test set objects. Objects were ranked according to the percent reduction in mean error for Mean over Puffball estimator. From top to bottom: 0, 25, 50, 75, and 100 percentile objects.

Since this limitation is a direct consequence of orthographic projection, an obvious next step is to use perspective projection, which will disambiguate these metamers and allow us to do a fairer comparison.

Even with statistically optimal estimators, given only elliptical approximations, shape and pose estimation is quite unreliable. The value of this work thus lies not in immediate application, but rather in the integration of these estimators with additional boundary shape cues as well as weak surface cues (e.g., shading, texture) that are usually present in the image but often insufficient to fully constrain 3D reconstruction.

## REFERENCES


Barron, J. T. and Malik, J. (2015). Shape, illumination, and reflectance from shading. *IEEE Transactions on Pattern Analysis and Machine Intelligence*, 37(8):1670–1687.

Besl, P. J. and McKay, H. D. (1992). A method for registration of 3-d shapes. *IEEE Transactions on Pattern Analysis and Machine Intelligence*, 14(2):239–256.

Blum, H. (1973). Biological shape and visual science (Part I). *J. Theor. Biol.*, 38:205–287.

Çalli, B., Walsman, A., Singh, A., Srinivasa, S., Abbeel, P., and Dollar, A. M. (2015). Benchmarking in manipulation research: The YCB object and model set and benchmarking protocols. *ArXiv e-prints*.

Cole, F., Isola, P., Freeman, W., Durand, F., and Adelson, E. (2012). Shapecollage: Occlusion-aware, example-based shape interpretation. In Fitzgibbon, A., Lazebnik, S., Perona, P., Sato, Y., and Schmid, C., editors, *Computer Vision ECCV 2012*, volume 7574 of *Lecture Notes in Computer Science*, pages 665–678. Springer Berlin Heidelberg.

Elder, J. H. (2014). Bridging the dimensional gap: Perceptual organization of contour into two-dimensional shape. In Wagemans, J., editor, *Oxford Handbook of Perceptual Organization*, Oxford, UK. Oxford University Press.

Freeman, W. T. (1994). The generic viewpoint assumption in a framework for visual perception. *Nature*, 368(6471):542–545.

Igarashi, T., Matsuoka, S., and Tanaka, H. (1999). Teddy: a sketching interface for 3D freeform design. In *Proceedings of the 26th annual conference on computer graphics and interactive techniques*, SIGGRAPH '99, pages 409–416, New York, NY, USA. ACM Press/Addison-Wesley Publishing Co.

Karsch, K., Liao, Z., Rock, J., Barron, J. T., and Hoiem, D. (2013). Boundary Cues for 3D Object Shape Recovery. In *Computer Vision and Pattern Recognition (CVPR), 2013 IEEE Conference on*, pages 2163–2170.

Koenderink, J. (1984). What does the occluding contour tell us about solid shape? *Perception*, 13(321-330).

Oswald, M., Toppe, E., Kolev, K., and Cremers, D. (2009). Non-parametric single view reconstruction of curved objects using convex optimization. In Denzler, J., Notni, G., and Süe, H., editors, *Pattern Recognition*, volume 5748 of *Lecture Notes in Computer Science*, pages 171–180. Springer Berlin Heidelberg.

Prasad, M., Zisserman, A., and Fitzgibbon, A. W. (2006). Single view reconstruction of curved surfaces. In *Computer Vision and Pattern Recognition, 2006 IEEE Computer Society Conference on*, volume 2, pages 1345–1354.

Singh, A., Sha, J., Narayan, K. S., Achim, T., and Abbeel, P. (2014). Bigbird: A large-scale 3D database of object instances. In *2014 IEEE International Conference on Robotics and Automation (ICRA)*, pages 509–516.

Todd, J. (2004). The visual perception of 3D shape. *Trends in Cognitive Sciences*, 8(3):115–121.

Todd, J. T. and Reichel, F. D. (1989). Ordinal structure in the visual perception and cognition of smoothly curved surfaces. *Psychological Review*, 96(4):643–657.

Toppe, E., Oswald, M. R., Cremers, D., and Rother, C. (2011). Image-based 3D Modeling via Cheeger Sets. In *Proceedings of the 10th Asian Conference on Computer Vision - Volume Part I*, ACCV'10, pages 53–64, Berlin, Heidelberg. Springer-Verlag.

Tse, P. (2002). A contour propagation approach to surface filling-in and volume formation. *Psychological Review*, 109(1):91–115.

Twarog, N. R., Tappen, M. F., and Adelson, E. H. (2012). Playing with Puffball: Simple scale-invariant inflation for use in vision and graphics. In *Proceedings of the ACM Symposium on Applied Perception*, SAP '12, pages 47–54, New York, NY, USA. ACM.